Hindawi Publishing Corporation
ISRN Mechanical Engineering
Volume 2013, Article ID 578072, 15 pages
http://dx.doi.org/10.1155/2013/578072

Research Article

Numerical Investigation of a First Stage of a Multistage Centrifugal Pump: Impeller, Diffuser with Return Vanes, and Casing

Nicolas La Roche-Carrier, Guyh Dituba Ngoma, and Walid Ghie

University of Quebec in Abitibi-Témiscamingue, School of Engineering's Department, 445 Boulevard de l'Université, Rouyn-Noranda, QC, Canada J9X 5E4

Correspondence should be addressed to Walid Ghie; walid.ghie@uqat.ca

Received 4 April 2013; Accepted 4 May 2013

Academic Editors: A. A. Kendoush, A. Z. Sahin, and Z. Yu

This paper deals with the numerical investigation of a liquid flow in a first stage of a multistage centrifugal pump consisting of an impeller, diffuser with return vanes, and casing. The continuity and Navier-Stokes equations with the k-ε turbulence model and standard wall functions were used. To improve the design of the pump's first stage, the impacts of the impeller blade height and diffuser vane height, number of impeller blades, diffuser vanes and diffuser return vanes, and wall roughness height on the performances of the first stage of a multistage centrifugal pump were analyzed. The results achieved reveal that the selected parameters affect the pump head, brake horsepower, and efficiency in a strong yet different manner. To validate the model developed, the results of the numerical simulations were compared with the experimental results from the pump manufacturer.

1. Introduction

Nowadays, multistage centrifugal pumps are widely used in industrial and mining enterprises. One of the most important components of a multistage centrifugal pump is the impeller (Peng [1]). The performance characteristics related to the pump including the head, brake horsepower, and efficiency rely heavily on the impeller. For a more performing multistage pump, its design parameters, such as the number of stages, impeller blades, diffuser vanes and diffuser return vanes, angle of the impeller blade, height of the impeller blade and diffuser vane, the width of the impeller blade and diffuser vane, the impeller and diffuser diameter, the rotating speed of the impeller, and the casing geometry must be determined accurately. Moreover, a stage of a multistage centrifugal pump is composed of an impeller, diffuser, and casing. Given the three-dimensional and turbulent liquid flow in a multistage centrifugal pump, it is very important to be aware of the liquid flow's behavior when flowing through a pump stage accounting for the wall roughness. This can be achieved by taking all stage components into consideration in the planning, design, and optimization phases in design and off-design conditions.

Many experimental and numerical studies have been conducted on the liquid flow through a single centrifugal pump (Cheah et al. [2], Ozturk et al. [3], Li [4], Liu et al. [5], González et al. [6], Asuaje et al. [7], and Kaupert and Staubli [8]) and a multistage centrifugal pump (Huang et al. [9], Miyano et al. [10], Kawashima et al. [11], and Gantar et al. [12]), where Cheah et al. [2] had numerically investigated the complex pump internal flow field in a centrifugal pump in design and off-design conditions using a CFD code. From the numerical simulation, it was found that the impeller passage flow at the design point was quite smooth and followed the blade curve; however, flow separation was observed at the leading edge due because the inflow was not tangential. Moreover, Ozturk et al. [3] had numerically investigated using a CFD code the impacts of the flow behavior in a centrifugal pump whose diffuser was subjected to different radial gaps were investigated. When the gap ratio decreased, it was shown that the jet was influenced within the diffuser because of the flow squeezing in small gap areas. Also, pump efficiency was

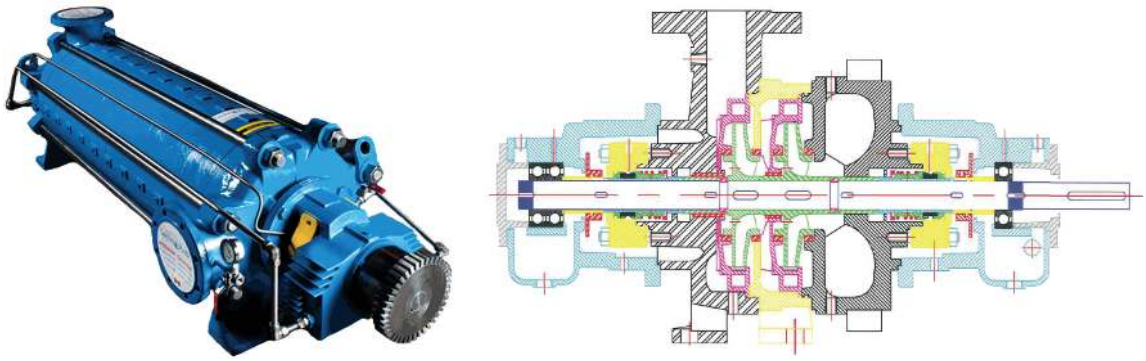

(a) 10-stage pump (b) Cross-sectional view of 2-stage pump

Figure 1: Typical multistage centrifugal pump [13].

(a) Centrifugal pump stage (b) Stage components

Figure 2: Model of a centrifugal pump stage.

only slightly affected by the impeller-diffuser gap distance, which decreased in the design flow conditions. In addition, Li [4], and Liu et al. [5] had experimentally examined the impacts of the number of impeller blades on the pump's performances. Furthermore, González et al. [6] had investigated numerically using a CFD code the dynamic impacts stemming from the impeller-volute interaction within a centrifugal pump, whereas the impacts of the volute on the velocity and pressure fields were examined by Asuaje et al. [7] and Kaupert and Staubli [8]. Furthermore, Huang et al. [9] had numerically simulated using a CFD code a three-dimensional turbulent flow through an entire stage of a multistage centrifugal pump, including flows in a rotating impeller and stationary diffuser. They had found that the reverse flows existed near the impeller outlet, resulting in the flow field being asymmetric and unstable. There was considerable interference on the velocity field at the impeller exit because of the interaction between the impeller blades and diffuser vanes. Additionally, Miyano et al. [10] had experimentally investigated the impacts of the return vane profile on the performances of the multistage centrifugal pump to optimize the stationary components in the multistage centrifugal pump. It was found, among other things, that the return vane, whose trailing edge was set at the outer wall radius of the downstream annular channel and discharged the swirl-less flow, had a positive impact on pump performances, while Kawashima et al. [11] had experimentally investigated the impacts of the diffuser vane on the performances of the multistage centrifugal pump, accounting for the interactions among the diffuser vane, return vane, and next stage impeller. The relevance in matching the diffuser vane and return vane properly to improve the pump efficiency of the multistage centrifugal pump was shown. It was also found that the efficiency could be improved by making the cross-sectional area of the channel from the diffuser vane outlet to the return vane inlet as large as possible. Moreover, Gantar et al. [12] had experimentally examined the multistage pump problems in conjunction with the axial thrust. The Laser Doppler Anemometry (LDA) was used to determine the fluid rotation in the impeller side chamber and its impact on the impeller hydraulic axial thrust for different leakage flow regimes. Moreover, the influence of the increased wear ring radial clearance on the axial thrust was analyzed with the solution for pump hydraulic axial thrust reduction.

Thorough analysis of previous works clearly demonstrated that the research results obtained are specific to the design parameters and configuration of the rotating and stationary components in single centrifugal pumps and multistage centrifugal pumps and thus cannot always be generalized. Therefore, in this study, to enhance the design and performances of multistage centrifugal pumps as shown in Figure 1, accounting for the particularities of the geometry

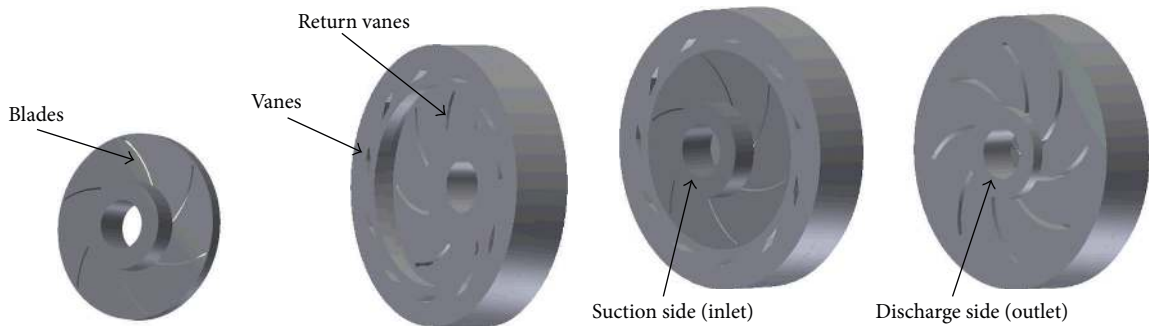

(a) Impeller (b) Diffuser (c) Stage: combined impeller and diffuser

Figure 3: Domain fluids of the stage components.

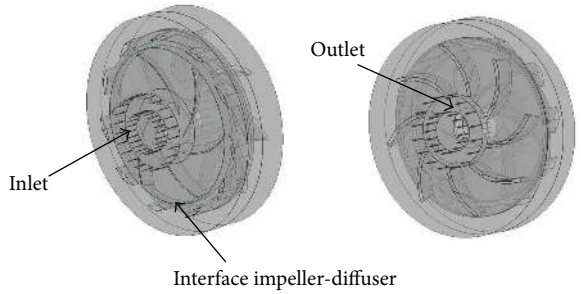

Figure 4: Domains of inlet, outlet, and interface.

and configuration of the impeller and diffuser with return vanes, a numerical investigation was conducted using the ANSYS-CFX code (Ansys Inc. [14]). This was done to gain further insight into the characteristics of the three-dimensional turbulent liquid flow through a stage of a multistage centrifugal pump while also considering various flow conditions and pump design parameters including the heights of the impeller blade and diffuser vane (16 mm, 23 mm, and 29 mm); the numbers of impeller blades (5, 6 and 7); the number of diffuser vanes (7, 8, and 12); the number of diffuser return vanes (3, 8, and 11); and the height of the wall roughness (0 mm, 0.002 mm, and 2 mm) for the impeller, diffuser, and inner casing wall. Upon applying the continuity and Navier-Stokes equations, the liquid flow velocity and liquid pressure distributions in a pump stage were determined while accounting for boundary conditions and considering a constant rotating speed for the impeller. The pump stage head, brake horsepower, and efficiency were represented as a function of the volume flow rate, where the objective was to identify the values of selected design parameters that might improve pump stage performances with respect to their value ranges.

2. Mathematical Formulation

The model of a first stage of the multistage centrifugal pump considered in this study is shown in Figure 2. It consists of an impeller, diffuser with return vanes and casting. The diffuser return vane passages are composed of the back diffuser wall, back diffuser vanes, and casing wall.

To run the numerical simulations, the used domain fluids of the impeller and diffuser with return vanes are shown in Figure 3.

In the centrifugal pump stage's governing equations for liquid flow, the following assumptions were made: (i) a steady-state, three-dimensional, and turbulence flow using the k-ε model was assumed; (ii) it was an incompressible liquid; (iii) it was a Newtonian liquid; and (iv) the liquid's thermophysical properties were constant with the temperature.

To account for these assumptions, the theoretical analysis of the liquid flow in the impeller passages, diffuser vane passages, and diffuser return vane passages was based on the continuity and Navier-Stokes [14] equations. For the three-dimensional liquid flow through these components of a centrifugal pump stage as shown in Figure 3, the continuity equations are expressed by

$$\nabla \cdot \vec{V}_{\text{vel}} = 0, \tag{1}$$

where $\vec{V}_{\text{vel}} = \vec{V}_{\text{vel}}(u(x, y, z), v(x, y, z), w(x, y, z))$ is the liquid flow velocity vector.

Using the coordinate system, (1) can be rewritten as

$$\frac{\partial u}{\partial x} + \frac{\partial v}{\partial y} + \frac{\partial w}{\partial z} = 0, \tag{2}$$

and the Navier-Stokes equations are given by

$$\begin{aligned} &\rho \nabla \cdot \left(\vec{V}_{\text{vel}} \otimes \vec{V}_{\text{vel}}\right) \\ &\quad = -\nabla p + \mu_{\text{eff}} \nabla \cdot \left(\nabla \vec{V}_{\text{vel}} + \left(\nabla \vec{V}_{\text{vel}}\right)^{T}\right) + B, \end{aligned} \tag{3}$$

where p is the pressure, ρ is the density, μ_{eff} is the effective viscosity accounting for turbulence, $\otimes$ is a tensor product, and B is the source term. For flows in an impeller rotating at a constant speed ω, the source term can be written as follows:

$$B = -\rho \left(2\vec{\omega} x \vec{V}_{\text{vel}} + \vec{\omega} x \left(\vec{\omega} x \vec{r}\right)\right), \tag{4}$$

where $\vec{r}$ is the location vector, $2\vec{\omega} x \vec{V}_{\text{vel}}$ is the centripetal acceleration, and $\vec{\omega} x (\vec{\omega} x \vec{r})$ is the Coriolis acceleration.

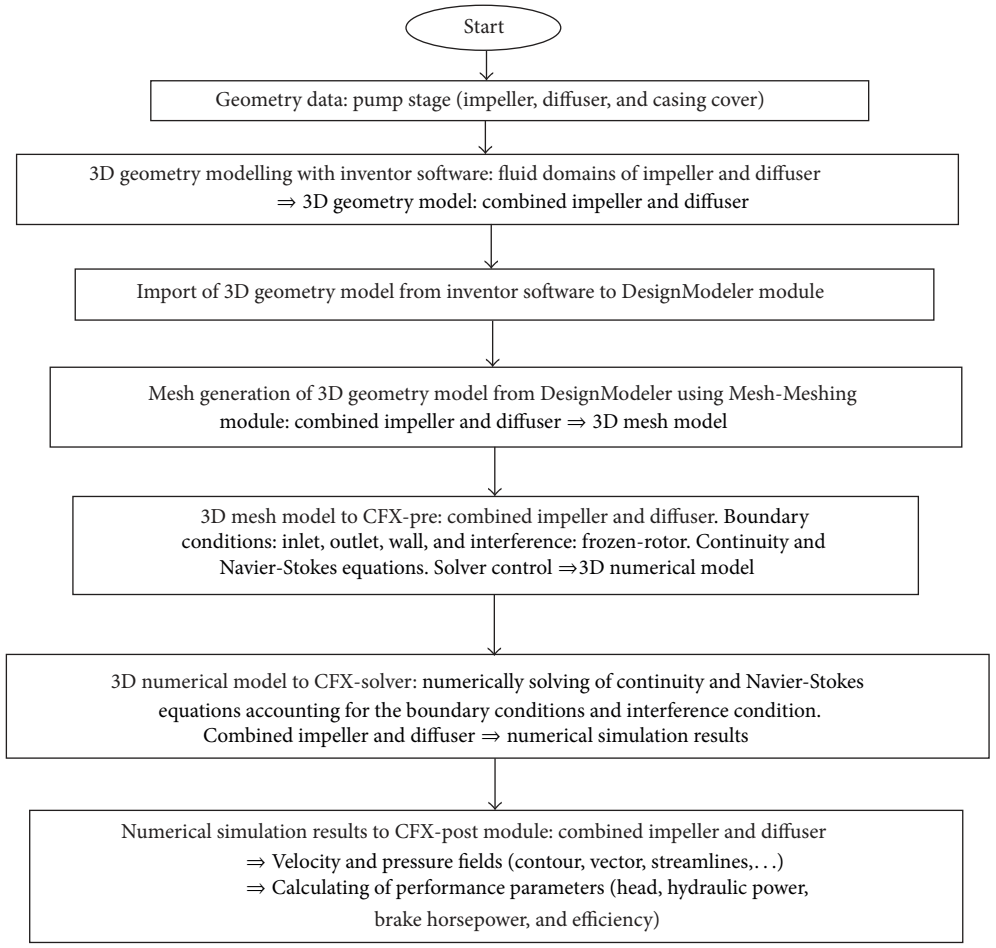

Figure 5: Steps from 3D geometry model to 3D numerical model and to numerical simulation results.

B is zero for the flow in the stationary components like the diffuser. Using the coordinate system, (3) can be rewritten as

$$\begin{aligned}
&\rho\left(u\frac{\partial u}{\partial x}+v\frac{\partial u}{\partial y}+w\frac{\partial u}{\partial z}\right)\\
&\quad=-\frac{\partial p}{\partial x}+\mu_{\text{eff}}\left(\frac{\partial^2 u}{\partial x^2}+\frac{\partial^2 u}{\partial y^2}+\frac{\partial^2 u}{\partial z^2}\right)+B_x,\\
&\rho\left(u\frac{\partial v}{\partial x}+v\frac{\partial v}{\partial y}+w\frac{\partial v}{\partial z}\right)\\
&\quad=-\frac{\partial p}{\partial y}+\mu_{\text{eff}}\left(\frac{\partial^2 v}{\partial x^2}+\frac{\partial^2 v}{\partial y^2}+\frac{\partial^2 v}{\partial z^2}\right)+B_y,\\
&\rho\left(u\frac{\partial w}{\partial x}+v\frac{\partial w}{\partial y}+w\frac{\partial w}{\partial z}\right)\\
&\quad=-\frac{\partial p}{\partial z}+\mu_{\text{eff}}\left(\frac{\partial^2 w}{\partial x^2}+\frac{\partial^2 w}{\partial y^2}+\frac{\partial^2 w}{\partial z^2}\right)+B_z,
\end{aligned}\tag{5}$$

where

$$\begin{aligned}
B_x&=\rho\left(\omega_z^2 r_x+2\omega_z v\right),\\
B_y&=\rho\left(\omega_z^2 r_y-2\omega_z u\right),\\
B_z&=0.
\end{aligned}\tag{6}$$

Furthermore, μ_{eff} is defined as

$$\mu_{\text{eff}}=\mu+\mu_t,\tag{7}$$

where μ is the dynamic viscosity and μ_t is the turbulence viscosity.

Since the k-ε turbulence model is used in this work because convergence is better than with other turbulence models, μ_t is linked to turbulence kinetic energy k and dissipation ε via the following relationship:

$$\mu_t=C_\mu\rho k^2\varepsilon^{-1},\tag{8}$$

where C_μ is a constant.

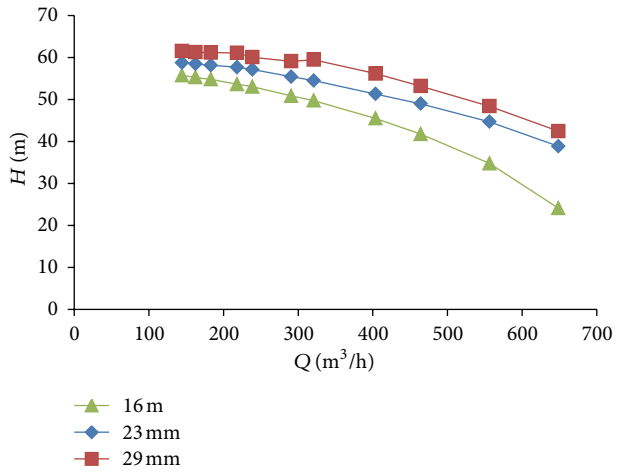

Figure 6: Pump stage head versus volume flow rate (parameter: blade height and vane height).

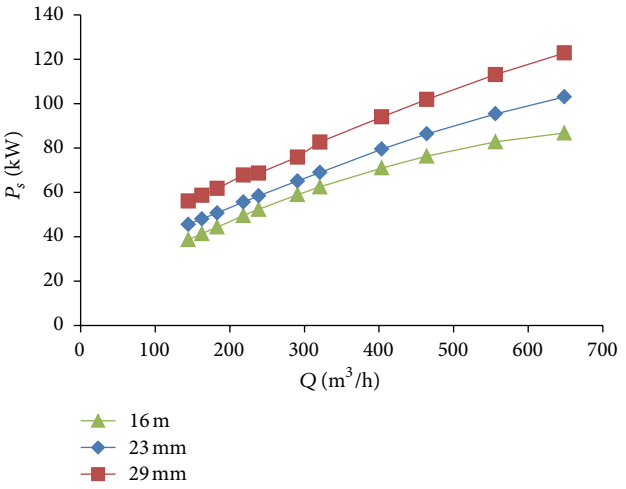

Figure 7: Brake horsepower versus volume flow rate (parameter: blade height and vane height).

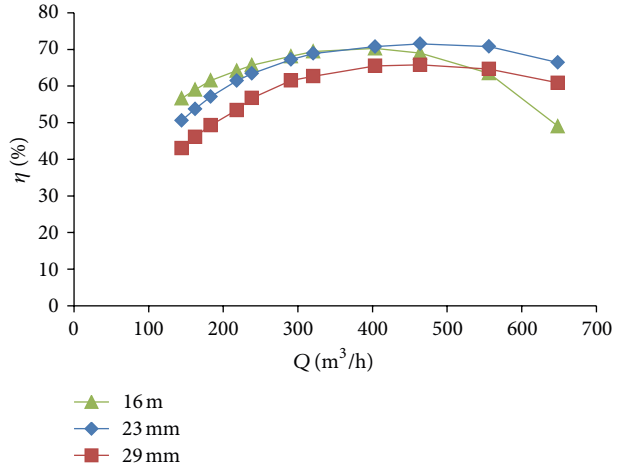

Figure 8: Efficiency versus volume flow rate (parameter: blade height and vane height).

The values for k and ε stem directly from the differential transport equations for turbulence kinetic energy and turbulence dissipation rates as follows:

$$\nabla \cdot \left(\rho \vec{V}_{\text{vel}} k\right) = \nabla \cdot \left[\left(\mu + \frac{\mu_t}{\sigma_k}\right) \nabla k\right] + p_k - \rho\varepsilon,$$
$$\nabla \cdot \left(\rho \vec{V}_{\text{vel}} \varepsilon\right) = \nabla \cdot \left[\left(\mu + \frac{\mu_t}{\sigma_\varepsilon}\right) \nabla \varepsilon\right] + \frac{\varepsilon}{k}\left(C_{\varepsilon 1} p_k - C_{\varepsilon 2} \rho\varepsilon\right), \tag{9}$$

where $C_{\varepsilon 1}$, $C_{\varepsilon 2}$, and σ_ε are constants. p_k is the turbulence production due to viscous and buoyancy forces, which is modeled using the following:

$$p_k = \mu_t \nabla \vec{V}_{\text{vel}} \cdot \left(\nabla \vec{V}_{\text{vel}} + \nabla \vec{V}_{\text{vel}}^{T}\right) - \frac{2}{3} \nabla \cdot \vec{V}_{\text{vel}} \left(3\mu_t \nabla \cdot \vec{V}_{\text{vel}} + \rho k\right) + p_{kb}, \tag{10}$$

$$p_{kb} = -\frac{\mu_t}{\rho \sigma_\rho} g \cdot \nabla \rho, \tag{11}$$

where p_{kb} can be neglected for the k-ε turbulence model.

Moreover, for the flow modeling near the wall, the logarithmic wall function is used to model the viscous sublayer [14].

To solve (2) and (5) numerically while accounting for the boundary conditions and turbulence model k-ε, the computational fluid dynamics ANSYS-CFX code, based on the finite volume method, was used to obtain the liquid flow velocity and pressure distributions. Pressure velocity coupling is calculated in ANSYS-CFX code using the Rhie Chow algorithm [14].

In the cases examined involving the pump stage, the boundary conditions were formulated as follows: the static pressure provided was given at the stage inlet (impeller inlet), while the flow rate provided was specified at the stage outlet (outlet of the diffuser return vane passage). The frozen rotor condition was used for the impeller-diffuser interface. A no-slip condition was set for the flow at the wall boundaries. Figure 4 shows the inlet, outlet, and interface domains for the selected pump stage, while the other domains were identified as the wall.

Furthermore, the ANSYS-CFX code includes the following modules: DesignModeler, Mesh-Meshing, CFX-pre, CFX-solver, and CFX-post. In Figure 5, the steps that were specifically used to obtain the numerical simulation results from the geometry models to the numerical model for the pump stage are depicted.

The pump stage head is formulated as follows:

$$H = \frac{p_{to} - p_{ti}}{\rho g}, \tag{12}$$

where p_{ti} is the total pressure at the pump stage inlet and p_{to} the total pressure at the pump stage outlet as shown in Figure 3. They are expressed as

$$p_{ti} = p_i + \frac{\rho}{2} V_{\text{vel}_i}^2, \qquad p_{to} = p_o + \frac{\rho}{2} V_{\text{vel}_o}^2. \tag{13}$$

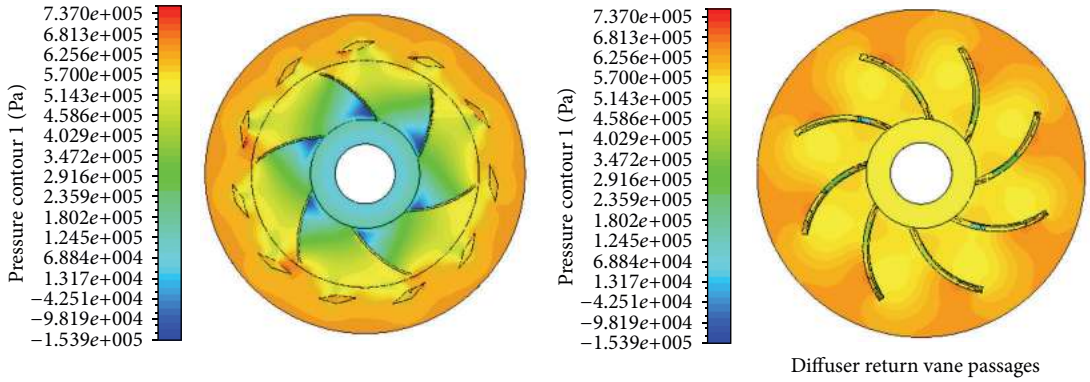

(a) Height = 16 mm and Δp = 407792 Pa

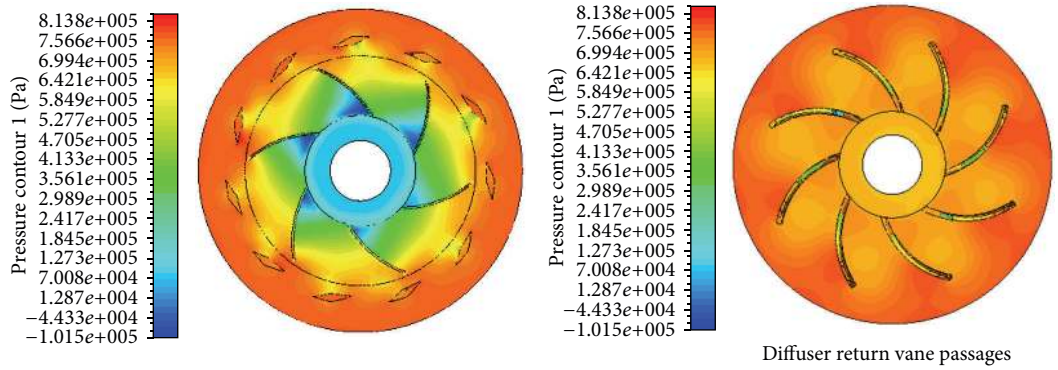

(b) Height = 23 mm and Δp = 479427 Pa

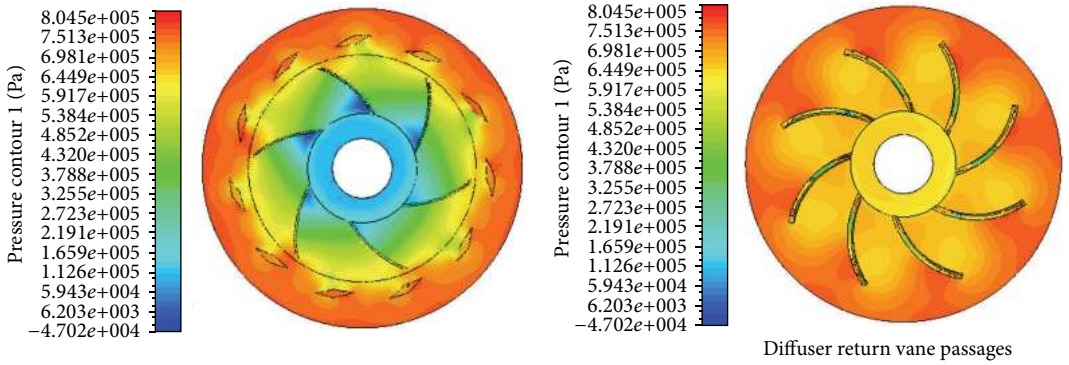

(c) Height = 29 mm and Δp = 519683 Pa

Figure 9: Static pressure contour.

Furthermore, the hydraulic power of the pump stage is given by

$$P_h = \rho Q g H, \tag{14}$$

where Q is the volume flow rate and H is the pump stage head.

In addition, the brake horsepower of the pump stage is expressed as follows:

$$P_s = C\omega, \tag{15}$$

where ω is the angular velocity and C is the impeller torque.

From the hydraulic power and the brake horsepower, the efficiency of the pump stage can be written as follows:

$$\eta = \frac{P_h}{P_s}. \tag{16}$$

The efficiency can also be formulated in terms of the hydraulic efficiency, η_h; the volumetric efficiencies, η_v; and mechanical efficiency, η_m, as:

$$\eta = \eta_h \eta_v \eta_m. \tag{17}$$

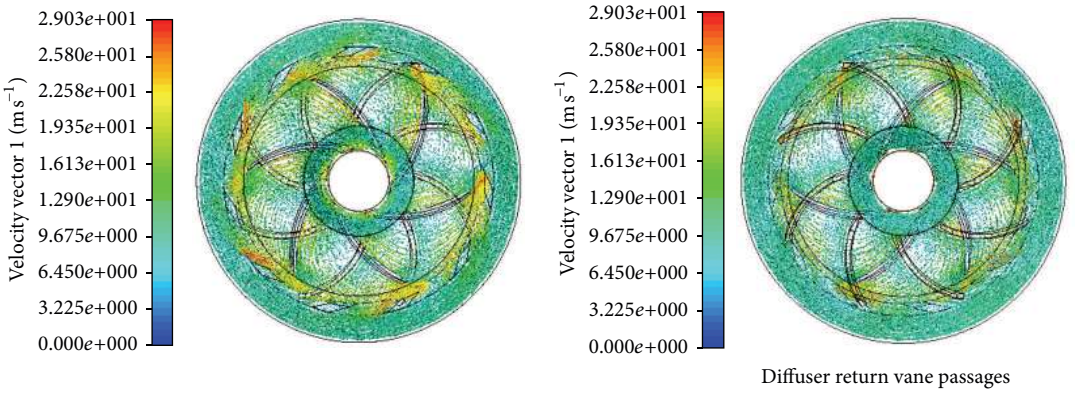

(a) Height = 16 mm

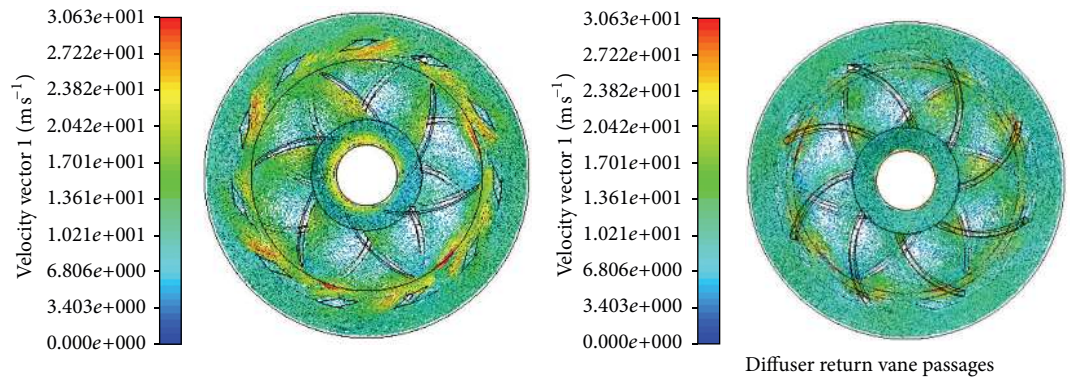

(b) Height = 23 mm

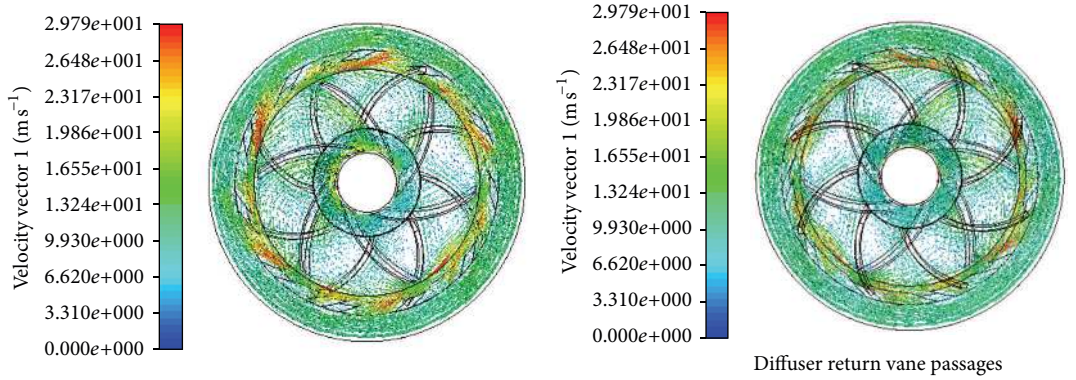

(c) Height = 29 mm

Figure 10: Liquid flow velocity vector.

3. Results and Discussion

Water was used as the working liquid for all simulation runs in this study and was considered to have the following reference values: temperature of 25°C for water, dynamic viscosity of $\mu = 8.899 \times 10^{-4}$ Pas, and density of $\rho = 997\,\text{kg/m}^3$. The main reference data for the impeller and diffuser appears in Table 1.

3.1. Case Studies. Five parameters of the first stage of a multistage centrifugal pump were selected for examination of their impacts mainly on pump performances: blade height and vane height for the impeller and diffuser, respectively, (16 mm, 23 mm, and 29 mm), number of impeller blades (5, 6, and 7), number of diffuser vanes (7, 8, and 12), number of diffuser return vanes (3, 8, and 11), and wall roughness height (0 mm, 0.002 mm, and 2 mm) for the impeller, diffuser with return vanes, and inner casing wall. The numerical simulation results presented in this work were obtained with the highest accuracy by conducting mesh-independent solution tests in each case study using different numbers of mesh elements.

3.1.1. Impact of the Height of Impeller Blades and Diffuser Vanes. To analyze the impact of the height of impeller blades

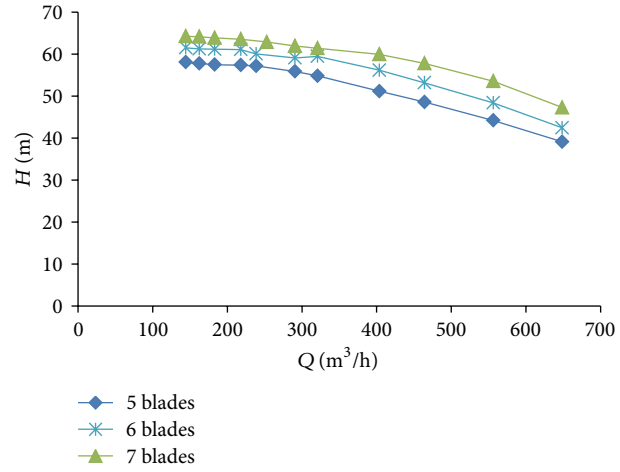

Figure 11: Pump stage head versus volume flow rate (parameter: blade number).

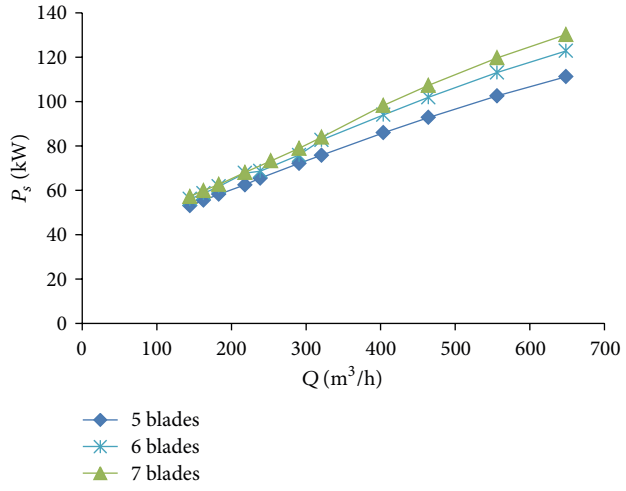

Figure 12: Brake horsepower versus volume flow rate (parameter: blade number).

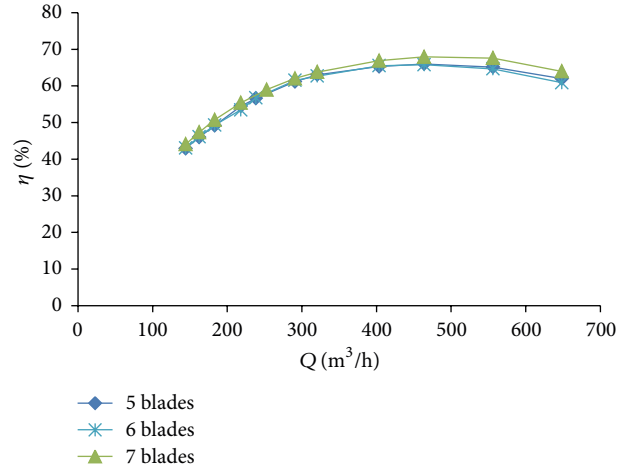

Figure 13: Efficiency versus volume flow rate (parameter: blade number).

Table 1: Main reference data for the impeller and diffuser.

m80Impeller		Diffuser	
Inner diameter (mm)	195	Inner diameter (mm)	407.016
Outer diameter (mm)	406	Outer diameter (mm)	571.5
Number of blades	6	Number of vanes	8
Rotating speed (rpm)	1750	Number of return vanes	11

and diffuser vanes on the pump stage head, brake horsepower and efficiency, the values of 16 mm, 23 mm, and 29 mm were selected for the impeller blade height and diffuser vane height, while keeping the other parameters constant. Figure 6 shows the pump stage head as a function of the volume flow rate with the blade height and vane height as a parameter, where it can be observed that the pump stage head decreases with an increasing volume flow rate due to decreasing liquid pressure. In addition, the pump stage head increases with increasing blade height and vane height. This is explained by the fact that when the volume flow rate is kept constant, the increased blade height leads to the decreasing meridional velocity, which increases the pump stage head, since the outlet tangential velocity and outlet blade angle remain constant. In other words, the liquid pressure drops in the impeller, and the diffuser decreases as a function of the increase in the blade height and vane height.

The curves expressing the pump stage brake horsepower as a function of the volume flow rate are shown in Figure 7, illustrating that the brake horsepower increases with increasing volume flow rate. This can be explained by the additional decrease in liquid pressure relative to the volume flow rate. Also, the brake horsepower increases relative to the impeller blade height due to the requested increase in pump shaft torque relative to the increased blade height.

The curves representing pump stage efficiency as a function of the volume flow rate is depicted in Figure 8, where it is observed that the efficiency for the blade height and vane height of 16 mm decreases rapidly to the right of the best efficiency point (BEP). The efficiency of the blade height and vane height of 23 mm is highest at large volume flow rates, whereas the efficiency of the blade height and vane height of 29 mm is lowest at volume flow rates ranging between 150 m^3/h and 550 m^3/h.

Figures 9 and 10 show the corresponding contours for static pressure and liquid flow velocity vectors for $Q = 464\ m^3/h$. Figure 9 clearly shows that the static pressure increases with the increasing blade height and vane height. This is due mainly to the decrease in liquid flow velocity at the impeller outlet as depicted in Figure 10, where average liquid flow velocities at the impeller outlet decrease from 18.43 for 16 mm to 15.67 m/s for 29 mm. Also, the recirculation phenomenon is observed in the diffuser return vane passages. Furthermore, the distribution of pressure difference ($\Delta p = p_o - p_i$) in the stage components is presented in Table 2.

3.1.2. Impact of the Number of Impeller Blades. To investigate the impact of the number of impeller blades on

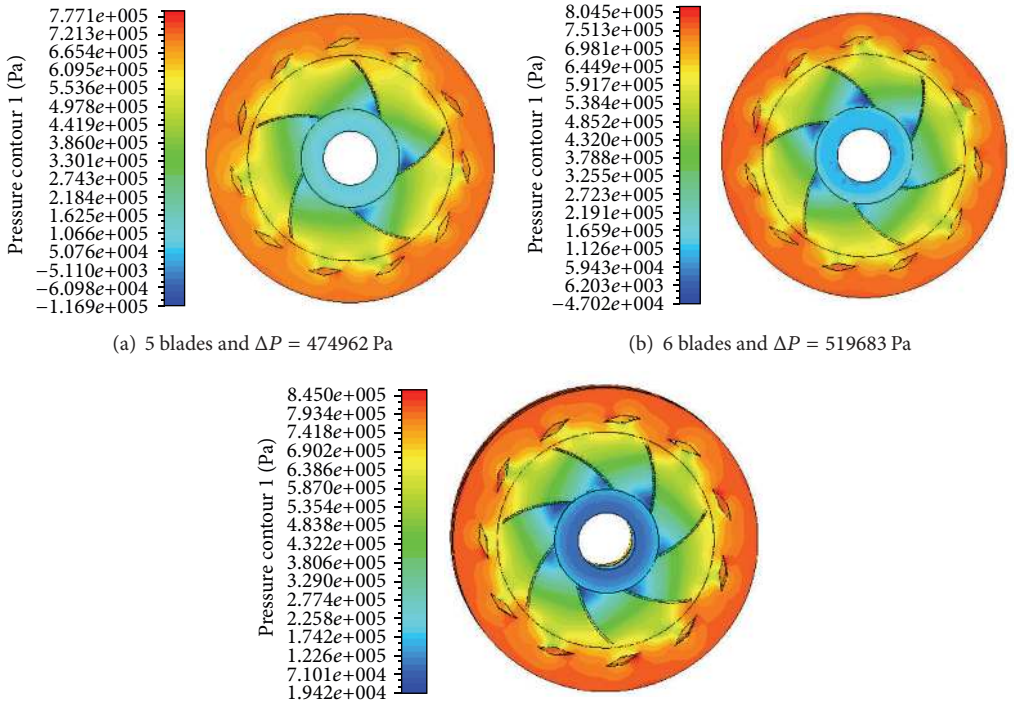

(a) 5 blades and $\Delta P = 474962$ Pa

(b) 6 blades and $\Delta P = 519683$ Pa

(c) 7 blades and $\Delta P = 564968$ Pa

Figure 14: Static pressure contour.

Table 2: Distribution of the pressure difference.

Blade or vane height	Pressure difference Δp Pa			
	Impeller	Diffuser	Diffuser return vane passages	Δp_{total}
16 mm	424908	74626	−91742	407792
23 mm	485468	92713	−98754	479427
29 mm	512751	108942	−102010	519683

Table 3: Distribution of pressure difference.

Blade number	Pressure difference Δp Pa			
	Impeller	Diffuser	Diffuser return vane passages	Δp_{total}
5	476784	98196	−100018	474962
6	512751	108942	−102010	519683
7	547270	120316	−102618	564968

the pump stage head, the brake horsepower, and efficiency, three impellers with 5, 6, and 7 blades were selected for a diffuser with 11 vanes and 8 return vanes, while the other parameters were kept constant. Figure 11 shows the head as a function of the volume flow rate, illustrating that the head and the static pressure keep increasing as the number of blades increases. Thus, the ideal head is produced when the number of impeller blades becomes infinite. Additionally, as shown in Figure 12, the brake horsepower increases relative to the increased number of impeller blades. This is due to the increase in the request pump shaft torque, as the number of impeller blades also increases.

Furthermore, Figure 13 shows the efficiency curves, showing that impellers with 5 and 6 blades are not as efficient as impellers with 7 blades for large volume flow rates.

Furthermore, Figure 13 shows the efficiency curves, showing that the impellers with 5 and 6 blades have the same efficiency that is lower than the efficiency for the impeller with 7 blades for large volume flow rates.

Moreover, Figures 14 and 15 depict the corresponding static pressure contour and liquid flow velocity vector for $Q = 464\ \text{m}^3/\text{h}$, respectively. These figures thus clearly show the increased static pressure difference between the stage outlet and impeller inlet relative to the increasing number of blades. This confirms the reduction in the liquid flow velocity at the impeller outlet relative to the greater number of blades, as represented in Figure 15, where the average liquid flow velocities at the impeller outlet were 18.13 m/s, 15.67 m/s, and 14.32 m/s for 5 blades, 6 blades, and 7 blades, respectively. In addition, the distribution of the pressure difference in the impeller, diffuser, and diffuser return vane passages is indicated in Table 3.

3.1.3. Impact of the Number of Diffuser Vanes. To analyze the impact that the number of diffuser vanes has on the pump stage head, brake horsepower, and efficiency, three diffuser models (with 7, 8, and 12 vanes, and 8 return vanes) were selected considering an impeller with 5 blades, while other parameters were kept constant. Figure 16 shows the head as a function of the volume flow rate, where it is observed that the head obtained with diffusers with 7 and 8 vanes is almost the

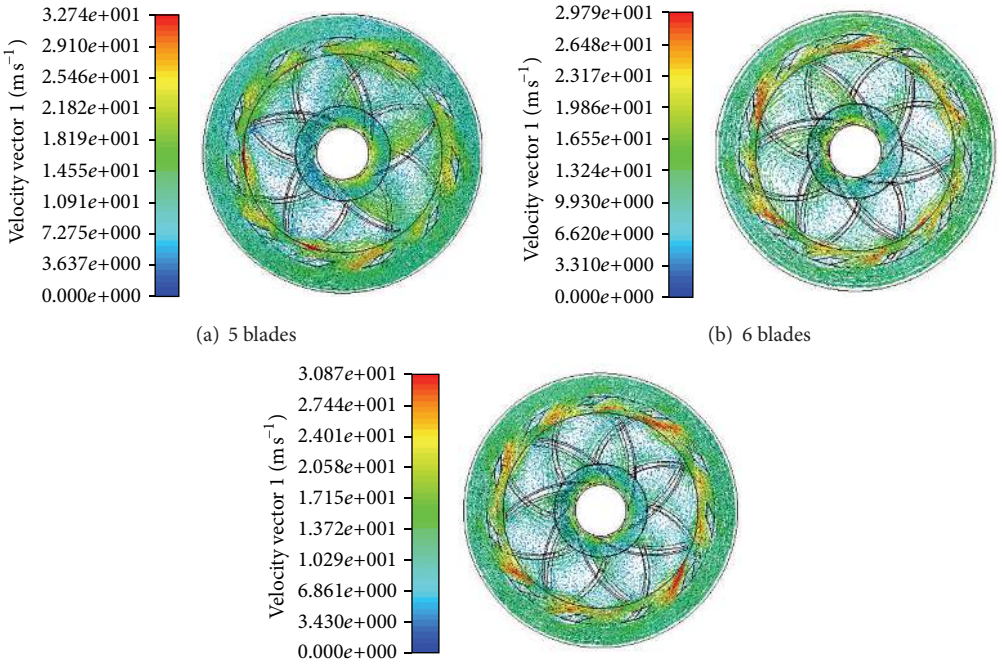

FIGURE 15: Vectors of liquid flow velocity contour.

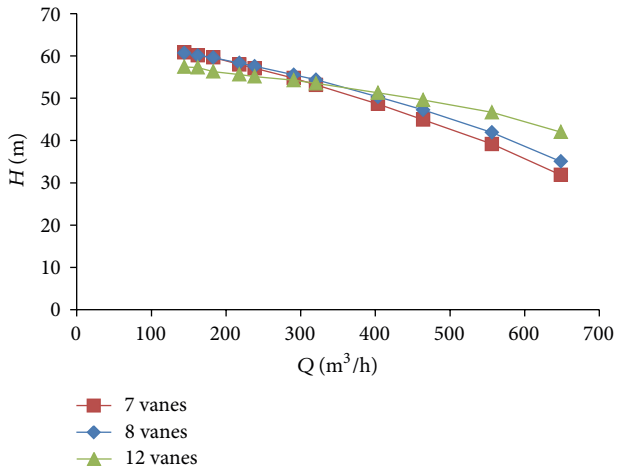

FIGURE 16: Pump stage head versus volume flow rate (parameter: vane number).

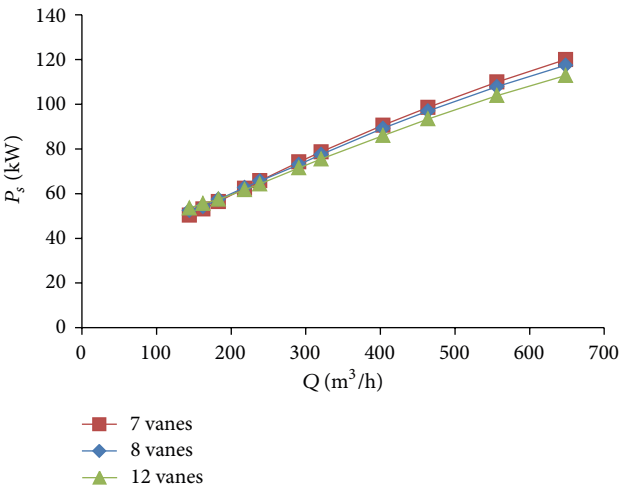

FIGURE 17: Brake horsepower versus volume flow rate (parameter: vane number).

same for a volume flow rate smaller than 320 m^3/h, whereas the head with the diffuser with 12 vanes is smallest. For large volume flow rates, the head with the diffuser with 12 vanes is the highest. This is due to a rise in static pressure through the reduction in flow velocity in a diffuser (diffusion effect). The flow guidance and friction effect depend on the number of diffuser vanes and the volume flow rate. When the number of diffuser vanes increases, the diffuser vane passages become narrower. This leads to better fluid guidance. In other words, flow loss decreases as the number of diffuser vanes increases. Friction loss increases with an increasing number of diffuser vanes. Furthermore, flow guidance, friction loss, and static pressure conversion are affected by the volume flow rate. Thus, there is an antagonistic impact between the diffusion impact and the friction loss in the range of the volume flow rate considered. As depicted in Figure 17, brake horsepower variation due to the number of diffuser blades is also small, even if the lowest brake horsepower is reached with 12 diffuser blades.

Furthermore, Figure 18 shows that for low and high volume flow rates, the efficiency of 12 diffuser vanes is highest,

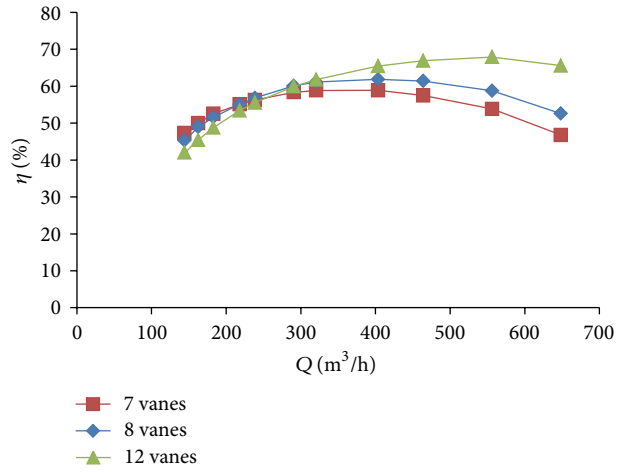

Figure 18: Efficiency versus volume flow rate (parameter: vane number).

Table 4: Distribution of pressure difference.

Vane number	Pressure difference Δp Pa			
	Impeller	Diffuser	Diffuser return vane passages	Δp_{total}
7	500556	70817	−89149	482224
8	496559	87279	−85170	498668
12	476198	103252	−78607	500843

whereas the efficiency for 7 and 8 diffuser vanes is nearly the same for a volume flow rate smaller than 320 m^3/h. This figure also indicates that the efficiency is lowest for 7 diffuser vanes for a volume flow rate higher than 320 m^3/h. Additionally, the best efficiency point (BEP) moves towards large volume flow rates and rises as the number of diffuser vanes increases.

Moreover, Figures 19 and 20 depict the corresponding static pressure contour and liquid flow velocity vector for Q = 403 m^3/h, respectively, showing that for these figures, there is a correlation between increased static pressure difference and decreased liquid flow velocity at the diffuser outlet, with an increased diffuser vane number. The average liquid flow velocity values at the diffuser outlet of 13.94 m/s, 13.14 m/s, and 11 m/s were found for 7, 8, and 12 vanes, respectively, as shown in Figure 20. Also, Table 4 indicates the pressure difference in the impeller, diffuser, and diffuser return vane passages.

3.1.4. Impact of the Number of Diffuser Return Vanes. To investigate the impact that the number of diffuser return vanes has on the pump stage head, brake horsepower, and efficiency, three diffuser models with 3, 8, and 11 return vanes and 11 vanes were selected considering an impeller with 6 blades, while other parameters were kept constant. Figure 21 shows the head as a function of the volume flow rate, where it is observed that the head obtained with the 3 diffuser return vanes is the lowest. This can be explained by the fact that the variation in the number of diffuser return vanes affects flow loss due to flow guidance and friction loss in diffuser return vanes. As depicted in Figure 22, the brake horsepower is only slightly affected by the number of diffuser return vanes.

Table 5: Distribution of pressure difference.

Return vane number	Pressure difference Δp Pa			
	Impeller	Diffuser	Diffuser return vane passages	Δp_{total}
3	517349	103444	−122147	498646
8	512751	108942	−102010	519683
11	516752	107500	−92048	532204

Table 6: Distribution of pressure difference.

Wall roughness height mm	Pressure difference Δp Pa			
	Impeller	Diffuser	Diffuser return vane passages	Δp_{total}
0	512751	108942	−102010	519683
2	486786	79951	−80182	486555

Furthermore, Figure 23 shows that for higher volume flow rates, the efficiency of the diffuser with 11 return vanes is highest. This figure also indicates that the efficiency is lowest for 5 diffuser vanes.

Additionally, Table 5 indicates the pressure difference in the impeller, diffuser, and diffuser return vane passages, where it can be observed that the highest pressure loss in the diffuser with 3 return vanes.

3.1.5. Impact of Wall Roughness Height. To investigate the impact of the wall roughness height of the impeller, diffuser and casting on the pump stage head, brake horsepower, and efficiency, three wall roughness heights (0 mm, 0.002 mm, and 2 mm) were chosen, while the other parameters were kept constant. Figure 24 shows the head as a function of the volume flow rate, where it is observed that the head is not affected by the value of the wall roughness height at 0 mm and 0.002 mm. On the contrary, it decreases when the wall roughness height increases further. This is explained by the fact that the friction loss rises with significantly increasing wall roughness height. In other words, the wall roughness increases the flow resistance in turbulent flow. This confirms that the casting process used for the impeller, diffuser, and casting has an impact on their surface finish, which influences the friction loss in flow passage and thus the head. As depicted in Figure 25, the brake horsepower increases with increasing wall roughness height for large volume flow rates due to the rising of friction loss with increasing wall roughness height for large volume flow rates. Thus, the requested pump torque increases.

Furthermore, Figure 26 shows the efficiency as a function of the volume flow rate, where it is observed that the efficiency is not influenced by the value of the wall roughness height for 0 mm and 0.002 m, while it decreases with the value of the wall roughness height at 2 mm due to the increase in friction loss. Moreover, the BEP moves towards a lower volume flow rate at the wall roughness height of 2 mm.

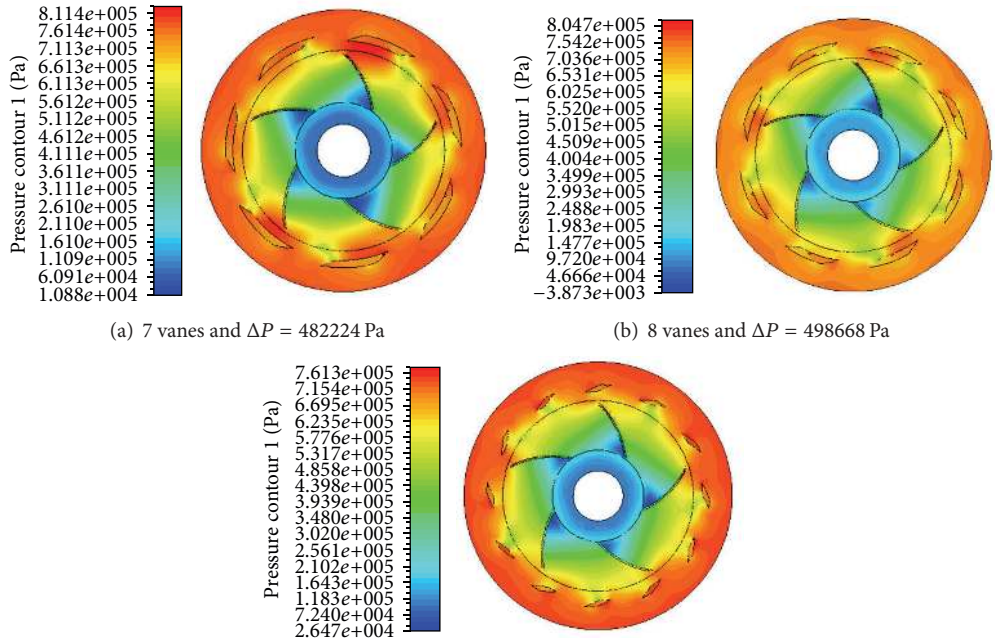

(a) 7 vanes and $\Delta P = 482224$ Pa

(b) 8 vanes and $\Delta P = 498668$ Pa

(c) 12 vanes and $\Delta P = 500843$ Pa

Figure 19: Static pressure contour.

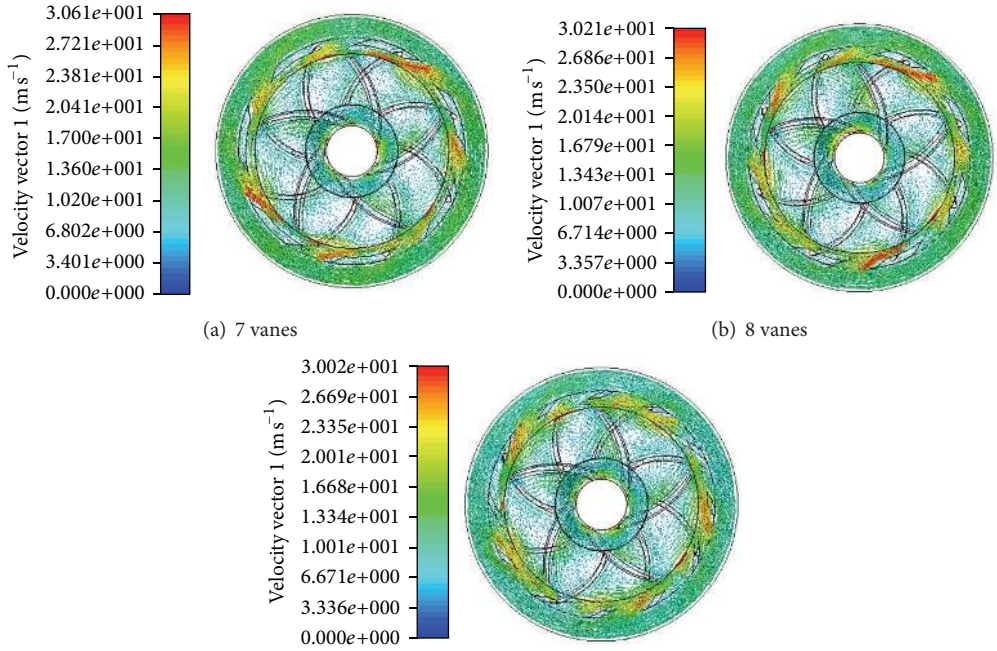

(a) 7 vanes

(b) 8 vanes

(c) 12 vanes

Figure 20: Vectors of liquid flow velocity.

Furthermore, Figure 27 depicts the corresponding static pressure contour for $Q = 464\,\text{m}^3/\text{h}$, which shows the distribution of static pressure in the impeller and diffuser with return vanes. Also, Table 6 presents the pressure differences in the impeller, diffuser and diffuser return vane passages obtained for the wall roughness heights of 0 mm and 2 mm. As previously mentioned, this clearly shows the decrease in total pressure difference with increasing wall roughness height.

3.2. Model Comparison. To validate the model developed for the first stage of a multistage centrifugal pump composed

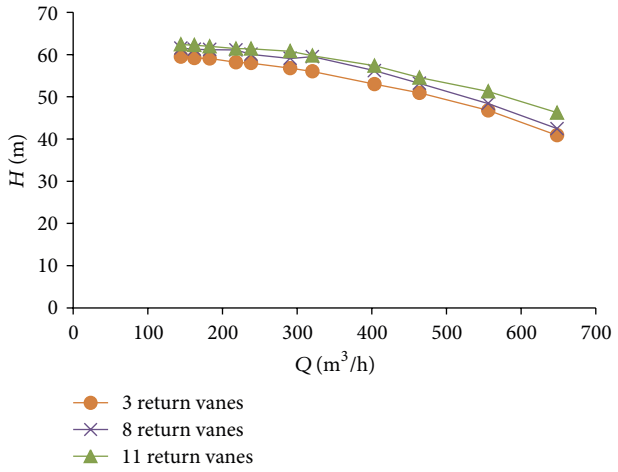

Figure 21: Pump stage head versus volume flow rate (parameter: return vane number).

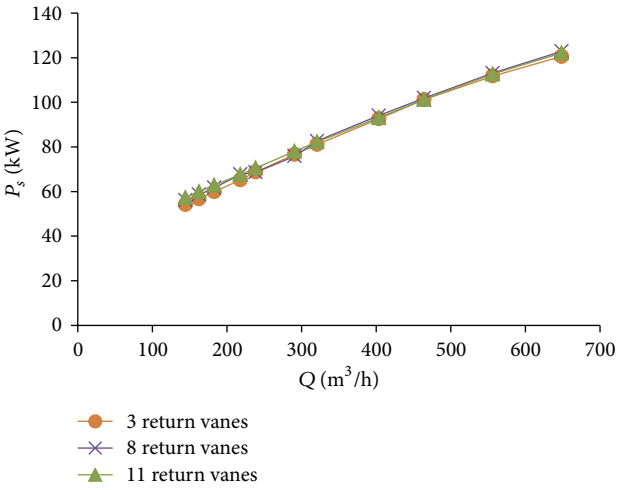

Figure 22: Brake horsepower versus volume flow rate (parameter: return vane number).

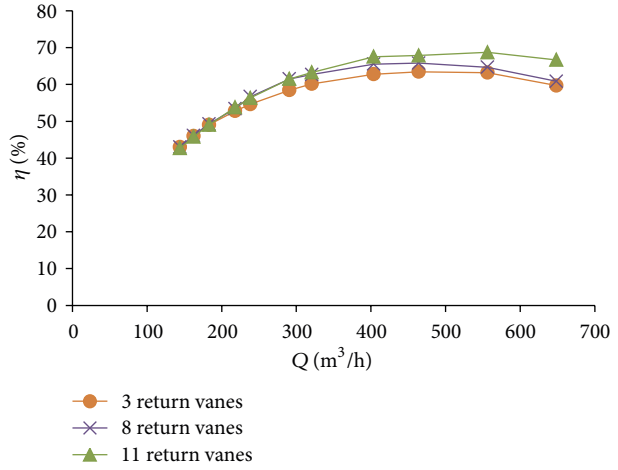

Figure 23: Efficiency versus volume flow rate (parameter: return vane number).

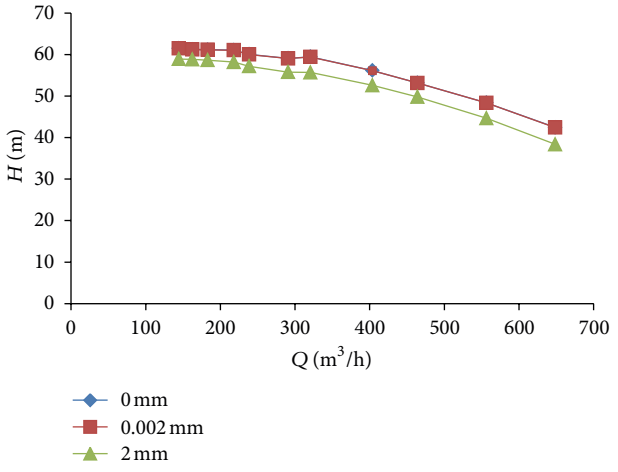

Figure 24: Pump stage head versus volume flow rate (parameter: wall roughness height).

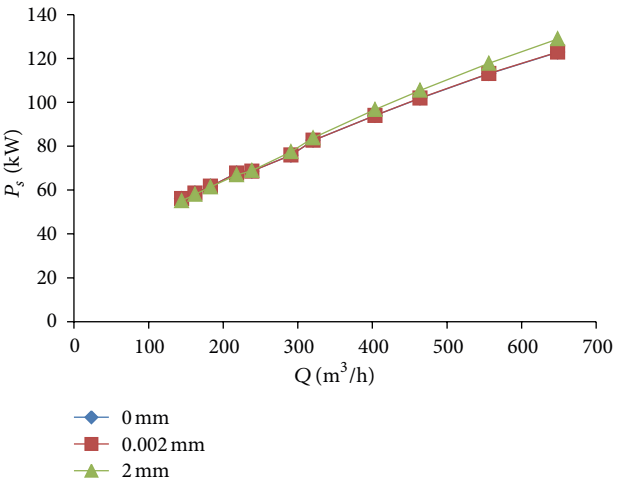

Figure 25: Brake horsepower versus volume flow rate (parameter: wall roughness height).

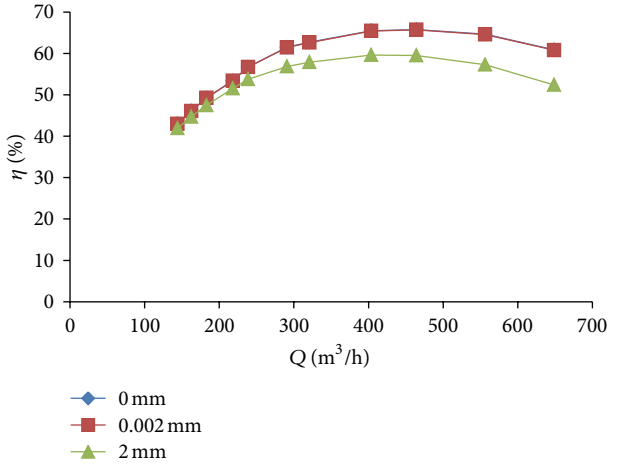

Figure 26: Efficiency versus volume flow rate (parameter: wall roughness height).

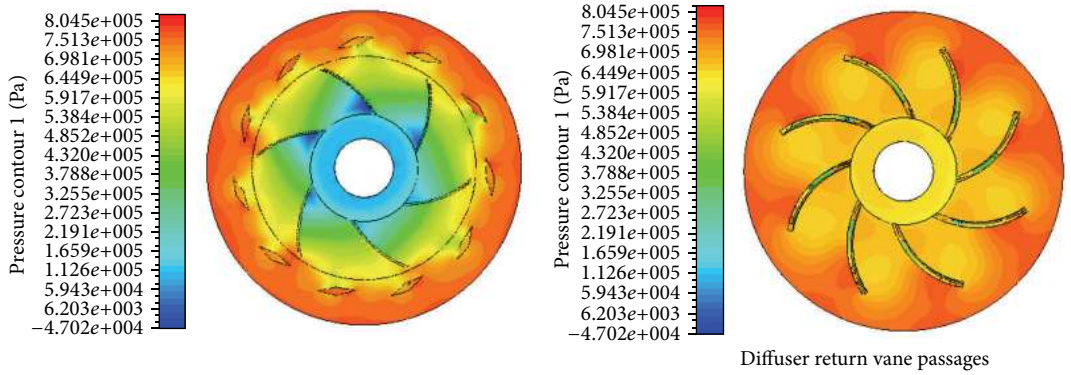

(a) 0 mm and $\Delta p = 519683$ Pa

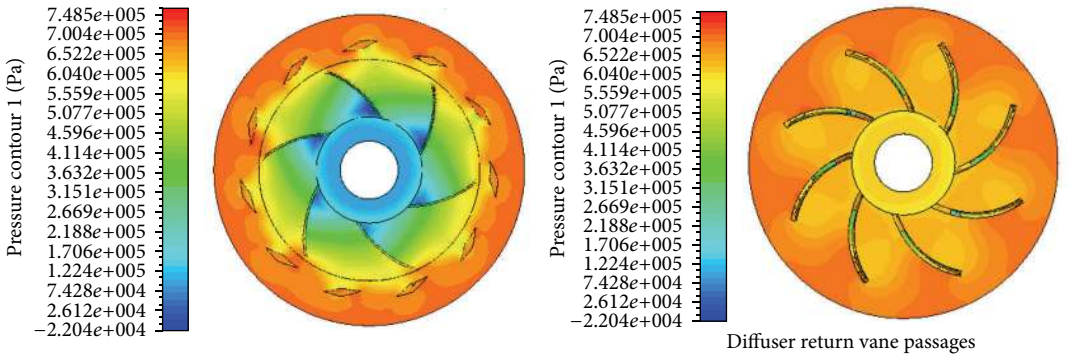

(b) 2 mm and $\Delta p = 486555$ Pa

Figure 27: Static pressure contour.

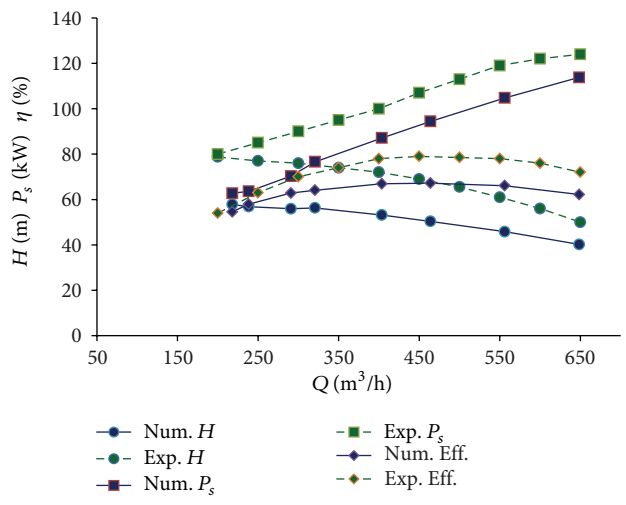

Figure 28: Comparison between the numerical results and experimental results.

of an impeller, diffuser with return vanes, and casting, the numerical simulation results were compared with the experimental results obtained from Technosub [13]. Figure 28 shows the comparison between the experimental and numerical curves for the head, brake horsepower, and efficiency. This comparison confirms that all the numerical curves follow the trend of the experimental curves.

The discrepancies observed can be explained, among other things, by the fact that the mechanical power loss and leakage power loss were not taken into account in the numerical simulations conducted. The values used for the mechanical efficiency and volumetric efficiency in the numerical simulations were as assumed to be constant; however, the additional parameters, which affect the gap between the numerical results and experimental results, are being more thoroughly investigated in the experimental and numerical sides to increasingly enhance the approach developed for the first stage of a multistage centrifugal pump.

4. Conclusion

In this study, a steady-state liquid flow in the three-dimensional first stage of a multistage centrifugal pump was numerically investigated. A model of a centrifugal pump stage composed of an impeller, diffuser, and casting was developed to analyze the impacts of the height of the impeller blades and diffuser vanes, the number of impeller blades, diffuser vanes and diffuser return vanes, and the wall roughness height on the pump stage head, brake horse power, and efficiency. The results obtained demonstrate, among other things, that the pump stage head and brake horsepower increase as the height of the impeller blades and diffuser vanes and the number of impeller blades increase. Moreover, the head and efficiency increase for large volume flow rates

with increasing numbers of diffuser vanes and diffuser return vanes. The brake horsepower hardly varies at all regardless of the number of diffuser vanes and diffuser return vanes. Furthermore, higher wall roughness heights of the impeller and diffuser negatively affect the head, brake horsepower, and efficiency. In all, the numerical curves obtained for the head, brake horsepower, and efficiency follow the trend of the experimental results.

Nomenclature

B: Sourceterm ($\mathrm{N\,m^{-3}}$)
C: Torque (N m)
g: Acceleration of gravity ($\mathrm{m\,s^{-2}}$)
H: Head (m)
P: Power (W)
p: Pressure ($\mathrm{N\,m^{-2}}$)
p_k: Turbulence production due to viscous and buoyancy forces
Q: Volume flow rate ($\mathrm{m^3\,s^{-1}}$)
r: Radial coordinate (m)
V: Velocity ($\mathrm{m\,s^{-1}}$)
u: Flow velocity in x direction ($\mathrm{m\,s^{-1}}$)
v: Flow velocity in y direction ($\mathrm{m\,s^{-1}}$)
w: Flow velocity in z direction ($\mathrm{m\,s^{-1}}$)
x: x-coordinate (m)
y: y-coordinate (m)
z: z-coordinate (m).

Greek Symbols

Δ: Difference
ε: Turbulence dissipation ($\mathrm{m^2\,s^{-3}}$)
η: Efficiency
k: Turbulence kinetic energy ($\mathrm{kg\,m^{-2}\,s^{-2}}$)
ρ: Fluid density ($\mathrm{kg\,m^{-3}}$)
μ: Dynamic viscosity (Pa s)
μ_{eff}: Effective viscosity (Pa s)
μ_t: Turbulence viscosity (Pa s)
ω: Angular velocity ($\mathrm{rad\,s^{-1}}$).

Subscripts

1: Inlet
2: Outlet
h: Hydraulic
i: Inlet
m: Mechanical
o: Outlet
s: Shaft
t: Total
v: Volumetric
vel: Velocity.

Acknowledgments

The authors are grateful to the Foundation of University of Quebec in Abitibi-Témiscamingue (FUQAT) and the company Technosub Inc.

References

[1] W. Peng, *Fundamentals of Turbomachinery*, John Wiley and Sons, Hoboken, NJ, USA, 2008.

[2] K. W. Cheah, T. S. Lee, S. H. Winoto, and Z. M. Zhao, "Numerical flow simulation in a centrifugal pump at design and off-design conditions," *International Journal of Rotating Machinery*, vol. 2007, Article ID 83641, 8 pages, 2007.

[3] A. Ozturk, K. Aydin, B. Sahin, and A. Pinarbasi, "Effect of impeller-diffuser radial gap ratio in a centrifugal pump," *Journal of Scientific and Industrial Research*, vol. 68, no. 3, pp. 203–213, 2009.

[4] W. G. Li, "Influence of the number of impeller blades on the performance of centrifugal oil pumps," *World Pumps*, no. 427, pp. 32–35, 2002.

[5] H. Liu, Y. Wang, S. Yuan, M. Tan, and K. Wang, "Effects of blade number on characteristics of centrifugal pumps," *Chinese Journal of Mechanical Engineering*, vol. 23, no. 6, pp. 742–747, 2010.

[6] J. González, J. Fernández, E. Blanco, and C. Santolaria, "Numerical simulation of the dynamic effects due to impeller-volute interaction in a centrifugal pump," *Journal of Fluids Engineering*, vol. 124, no. 2, pp. 348–355, 2002.

[7] M. Asuaje, F. Bakir, S. Kouidri, F. Kenyery, and R. Rey, "Numerical modelization of the flow in centrifugal pump: volute influence in velocity and pressure fields," *International Journal of Rotating Machinery*, vol. 2005, no. 3, pp. 244–255, 2005.

[8] K. A. Kaupert and T. Staubli, "The unsteady pressure field in a high specific speed centrifugal pump impeller—Part I: influence of the volute," *Journal of Fluids Engineering*, vol. 121, no. 3, pp. 621–626, 1999.

[9] S. Huang, M. F. Islam, and P. Liu, "Numerical simulation of 3D turbulent flow through an entire stage in a multistage centrifugal pump," *International Journal of Computational Fluid Dynamics*, vol. 20, no. 5, pp. 309–314, 2006.

[10] M. Miyano, T. Kanemoto, D. Kawashima, A. Wada, T. Hara, and K. Sakoda, "Return vane installed in multistage centrifugal pump," *International Journal of Fluid Machinery and Systems*, vol. 1, no. 1, pp. 57–63, 2008.

[11] D. Kawashima, T. Kanemoto, K. Sakoda, A. Wada, and T. Hara, "Matching diffuser vane with return vane installed in multistage centrifugal pump," *International Journal of Fluid Machinery and Systems*, vol. 1, no. 1, 2008.

[12] M. Gantar, D. Florjancic, and B. Sirok, "Hydraulic axial thrust in multistage pumps—origins and solutions," *Journal of Fluids Engineering*, vol. 124, no. 2, pp. 336–341, 2002.

[13] Technosub Inc, http://www.technosub.net/.

[14] Ansys inc. 2011. ANSYS-CFX (CFX Introduction, CFX Reference Guide, CFX Tutorials, CFX-Pre User's Guide, CFX-Solver Manager User's Guide, CFX-Solver Modeling Guide, CFX-Solver Theory Guide), release 14. 0, USA.